THE JOURNAL OF PHYSICAL CHEMISTRY B

Article

pubs.acs.org/JPCB

Morphology, Thermal Behavior, and Stability of Self-Assembled Supramolecular Tubules from Lysine-Based Surfactants

Rodrigo O. Brito, Isabel S. Oliveira, Maria J. Araújo, and Eduardo F. Marques*

Centro de Investigação em Química, Department of Chemistry and Biochemistry, University of Porto, Rua do Campo Alegre, s/n, 4169-007 Porto, Portugal

ABSTRACT: Synthetic amino acid-based surfactants possess versatile aggregation properties and are typically more biocompatible and biodegradable than surfactants with conventional headgroups. This opens the possibility of a myriad of specialty applications, namely in pharmaceutics, cosmetics, biomedicine, and nanotemplating chemistry. In this work, we have investigated the interfacial and self-assembling properties in aqueous medium of novel double-chained lysine-based surfactants, with particular focus on the behavior of the dodecyl derivative, 12Lys12. Upon cooling from dilute isotropic micellar solutions, this surfactant crystallizes into micrometer-sized tubular structures that induce gelation of the system. The tubules have been characterized in terms of morphology, assembly process, thermal behavior, and stability, by using differential scanning calorimetry, light and scanning electron microscopy, and deuterium NMR. Possible mechanisms for tubule assembly are discussed, on the basis of surfactant molecular shape, H-bonding and electrostatic interactions, and chirality effects.

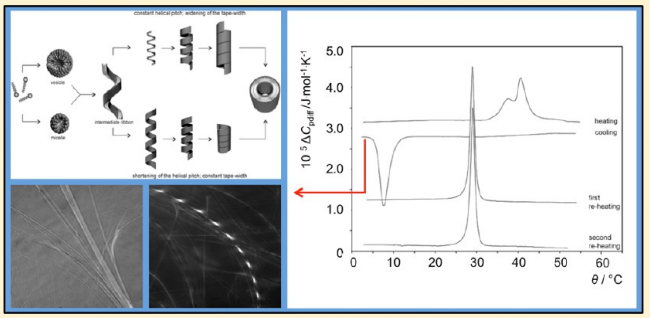

1. INTRODUCTION

The continuous technical demand for biofriendly high-performance amphiphiles has led to the synthesis and characterization of novel molecules derived from renewable natural motifs, such as sugars,[1,2] natural oils,[3] and amino acids.[4−6] These biocompatible surfactants find great potential for use *inter alia* in nanochemistry templating,[7,8] drug and gene delivery,[9−11] and gelation.[12−14] In particular, amino acid-based surfactants have emerged as a viable alternative to conventional surfactants due to their enhanced biodegradability,[5,15,16] low ecotoxicity,[17] and moderate human cytoxicity, which depends on alkyl chain length and headgroup chemistry.[18−20] Moreover, amino acid-based amphiphiles possess at least one chiral center (the amino acid chiral carbon) that may induce molecular packing into self-assembled tubular and filamentary structures.[21−23] The chiral center may also dictate a particular orientation of the molecules[4] and promote transitions between different aggregate structures, such as rods, fibers and ribbons.[12]

Several studies have focused on the application of tubular aggregates in drug delivery,[24,25] templating[7] and building block[26] nanochemistry, biosensors,[27] helical crystallization of proteins,[28] and rheological control of materials through gelation.[12,13,22,29] The gelation effect occurs by the entrapment of the solvent in a matrix typically built of a three-dimensional network of fibers and tubular structures stabilized by noncovalent interactions.[12,13]

With respect to chemical composition, supramolecular tubules can be assembled from a wide diversity of amphiphilic molecular motifs.[4] For instance, chiral nanoribbons and nanotubules have been obtained from gemini-tartrate amphiphiles.[30] Further tubule-forming amphiphiles are amino acid-derived surfactants,[23,31,32] peptides,[33] fatty acids,[34,35] trimethylammonium and sodium alkyl sulfate surfactants with amino acid and aromatic ions as counterions,[12,36] phospholipids,[37,38] sugar-derived surfactants,[39,40] bile salts,[41] and some amphiphilic polymers.[42,43]

In the current work, we report on the aggregation properties of novel anionic lysine-based surfactants (Figure 1), designated by

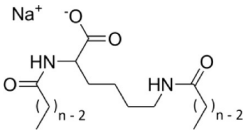

Figure 1. Molecular structure of the lysine-based surfactants studied in this work (n = 8, 10, and 12).

8Lys8, 10Lys10, and 12Lys12. These compounds are double-chained amphiphiles, with a pseudodimeric (i.e., pseudogemini) structure (Figure 1), and thus it is expected that they behave differently from single-chained amphiphiles. In a previous report, we have explored the thermotropic phase behavior of these compounds.[44] Recent studies on the synthesis and biological properties,[45] as well as pH studies and cytoxicity behavior,[46,47] of cationic lysine-based amphiphiles have also been reported.

Herein, special focus is placed on the formation of self-assembled tubules by 12Lys12 in water, using microscopy, calorimetry, and nuclear magnetic resonance as probing techniques. These tubular supramolecular structures form

Received: January 4, 2013
Revised: June 3, 2013
Published: June 19, 2013

spontaneously upon cooling of an isotropic micellar phase, show variable diameter, and are several micrometers long. To shed light on the aggregation behavior in the dilute regime, the main features of full-range phase behavior of these compounds have been also investigated, on the basis of phase scanning microscopy. The phase sequence found is common to all molecules: micellar phase, hexagonal phase, lamellar phase and hydrated crystals. Results show that chain length, pH, amphiphile concentration, hydrogen bonding and electrostatic interactions, and chirality, concur to determine tubule stabilization.

2. EXPERIMENTAL SECTION

2.1. Sample Preparation. The lysine-derived surfactants were synthesized and purified according to a previously described procedure.[31,48] Purity of the surfactants was ascertained by NMR and high resolution mass spectroscopy,[48] by DSC,[44] and also confirmed by the surface tension performed in this work (no dips in the vicinity of the *cmc* were found). The perdeuterated surfactant D12Lys12 was synthesized according to the same procedure, using a perdeuterated fatty acid, and purity was ascertained also by NMR and HRMS.

2.2. Surface Tension Measurements. A DCAT11 tensiometer from Dataphysics GmbH, with a Pt−Y alloy Wilhelmy plate, was used. The experiments were performed by adding aliquots from a stock surfactant solution to the measuring vessel. No dynamic surface tension effects were observed.

2.3. Light Microscopy. Phase scans of solid samples and high-contrast imaging of dilute aqueous dispersions were carried out with an Olympus BX51 light microscope, under polarized light mode and differential interference contrast (DIC) mode, respectively. Images were acquired with an Olympus C5060 video camera and software CellA. Samples for microscopic observations were prepared by dispersion of the solid surfactant in high purity Milli-Q water and sonicated in a Bandelin Sonorex sonication bath. For the thermal study of 12Lys12 dispersions, samples were loaded and sealed in 0.2 mm diameter glass capillaries provided by Vitrocom. Temperature was accurately controlled using a Linkam THMS600 heating stage (±0.1 °C). Phase scan samples were prepared by melting the solids in a glass slide and placing a cover glass on top of the thin film formed. The samples were allowed to relax at room temperature for 2 days before the hydration experiment.

2.4. Cryogenic Scanning Electron Microscopy (cryo-SEM). Cryogenic scanning electron microscopy imaging of the samples was done using a JEOL JSM 6301F scanning electron microscope, equipped with a Gatan Alto 2500 preparation chamber. A portion of a 0.5 wt % surfactant dispersion was applied on a copper sample-holder and fractured after vitrification in nitrogen slush from room temperature (20 °C).

2.5. Differential Scanning Calorimetry (DSC). DSC curves were obtained with a properly calibrated Setaram microDSC III calorimeter, at a scanning rate of 0.5 K·min^{-1}. Two steel batch cells were used, one containing the sample and the other neat water, as reference. Mass difference between the two cells was always lower than 0.1 mg.

2.6. Solid-State Nuclear Magnetic Resonance (NMR). Deuterium solid-state NMR experiments were performed at several temperatures from 20 to 70 °C on a 400 MHz Bruker spectrometer operating at 61 MHz for deuterium using a static double channel probe. The sample coil of the probe was adapted to load a 7 mm rotor such as those used for magic angle spinning probes equipped with a stretched stator. Typically, surfactant dispersions were previously heated to 70 °C and a volume of ca. 700 μL transferred into the rotor which was sealed and then end-capped. A Hahn quadrupolar echo sequence was used with an inter pulse delay of 40 μs. Eight thousand points in 1k accumulations (every 2 s) were done with a 90° pulse and spectral width of 8 μs and 250 kHz, respectively. Free induction decay signals were zero-filled to 16k points prior to Fourier transform after a broad line exponential multiplication of 100 Hz.

3. RESULTS AND DISCUSSION

3.1. Solution Behavior: Surface Tension Studies. All surface tension measurements of the aqueous solutions of lysine-based surfactant were carried out at pH = 12.0 ± 0.2, adjusted with NaOH 0.010 mol·dm^{-3}. This was done to suppress protolysis of the carboxylate group that could lead to formation of the insoluble acid form of the surfactant, especially at the initial low concentrations in the measuring vessel. Measurements were done at 25.0 °C for 8Lys8 and 10Lys10, because these surfactants are soluble at room temperature in the full concentration range explored, at that pH. For 12Lys12, measurements were done at 45.0 °C, as the Krafft temperature of the surfactant was found to be 43 °C by DSC (data below).

Figure 2a shows the surface tension vs ln(concentration) curves, which demonstrate that the surfactants follow a conventional micelle-forming behavior in water. No dips are visible, which implies absence of surface-active contaminants and

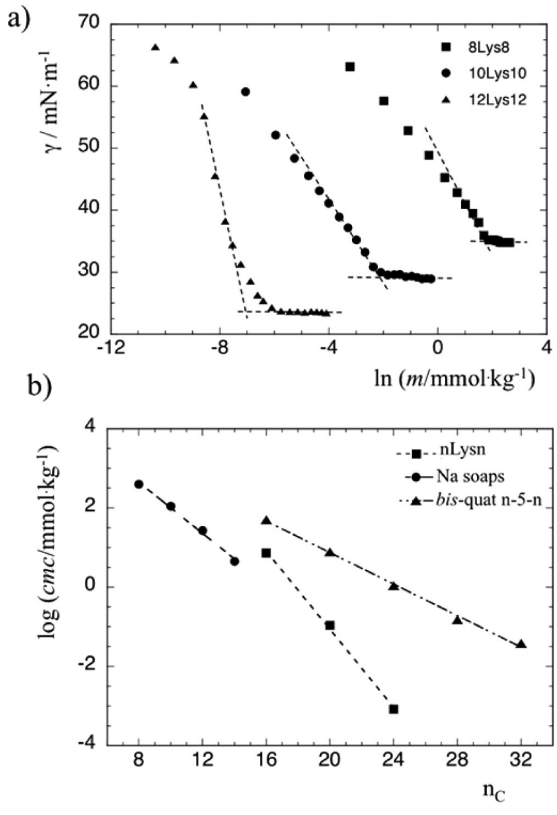

Figure 2. (a) Surface tension vs logarithm (concentration) graphs for the anionic lysine-based surfactants. (b) Logarithm of *cmc* vs total number of carbon atoms in the main hydrocarbon chains for nLysn (8Lys8, 10Lys10, and 12Lys12) surfactants (squares); sodium fatty soaps, with even chains from 8 to 14 (circles);[50] bis(quaternary ammonium) gemini surfactant with a 5-carbon spacer and main chains from 8 to 16 carbons (triangles), taken from Zana[49] and references therein cited.

dx.doi.org/10.1021/jp400127k | J. Phys. Chem. B 2013, 117, 9400−9411

Table 1. Interfacial Parameters Determined for the Anionic Lysine-Based Surfactants

surfactant	θ_{Kr}/°C	θ_{exp}/°C	cmc/mmol·kg^{-1}	γ_{cmc}/mN·m^{-1}	a_s/nm^2
8Lys8	<RT	25.0	7.3 ± 1.3	35.1	0.68 (1.36)
10Lys10	<RT	25.0	0.11 ± 0.06	28.5	0.59 (1.18)
12Lys12	43.0	45.0	(8.3 ± 0.2) × 10^{-4}	24.8	0.23 (0.46)

allows determination of reliable critical micelle concentration (cmc) values. Table 1 shows the different micellization parameters calculated from the curves, namely the cmc, the surface tension at the cmc, γ_{cmc}, and the minimum surface area per molecule, a_s. The maximum surface excess concentration, Γ_{max}, is calculated from the Gibbs adsorption equation:

$$\Gamma = -\frac{1}{nRT}\left(\frac{\partial\gamma}{\partial \ln m}\right)_{p,T} \quad (1)$$

where R is the ideal gas constant, T is the absolute temperature, $(\partial\gamma/\partial \ln m)$ is the slope of the γ−ln c plot just below cmc, m is the surfactant molal concentration, and n is the number of free species at the interface. The minimum surface area per molecule (a_s), at the air−water interface, is given by

$$a_s = \frac{1}{N_A\Gamma_{max}} \quad (2)$$

where N_A is the Avogadro constant.

As expected, the cmc and γ_{cmc} decrease with increasing chain length on account of the increasing hydrophobicity of the surfactants. Moreover, Figure 2b shows that, for the lysine surfactants, there is a linear dependence of log(cmc) with the number of carbon atoms in the main alkyl chains (slope −0.49), in line with the common behavior of other ionic surfactants. To some extent, nLysn compounds are structurally similar to gemini surfactants with a five-methylene spacer, the main difference being that, in the nLsyn compounds, one of the polar groups is uncharged (Figure 1). Thus, for comparison purposes, log(cmc) values for n-5-n bis(quaternary ammonium) gemini surfactants[49] are also shown (slope −0.20), as well for sodium alkylcarboxylates with 8−14 C atoms (slope −0.32).[50] Typical slope values of −0.3 for single-chained ionic surfactants indicate a factor of 2 decrease in cmc per added CH_2,[51] whereas the dependence is somewhat higher for the Lys surfactants (roughly factor of 3). This is likely due to the combined effect of the pseudogemini headgroup and double-chained structure of the Lys-based surfactants on cmc. The higher cmc values and weaker log(cmc) dependence on n_C for the bis-quat gemini, compared to the nLysn, can be attributed mainly to the presence of two charged headgroups, which turn the surfactants rather hydrophilic (and thus more soluble) despite their double-chained nature.

If one now compares the cmc of 12Lys12 (8.3 × 10^{-4} mmol·kg^{-1}) with the critical aggregation concentration of a homologous monomeric double-chained surfactant, like didodecyldimethylammonium bromide (DDAB, cac = 0.05 mmol·kg^{-1}),[52] the value is still lower for the former. This fact probably reflects weaker electrostatic polar repulsions in the micelles of 12Lys12 due to a bulkier headgroup than the quaternary ammonium headgroup of DDAB. In addition, and as would be expected, these double-chained Lys surfactants have cmc values somewhat lower than those of cationic surfactants based on the same amino acid, namely the acyl lysine methyl ester hydrochloride salts and gemini compounds reported by Perez et al.[46,47]

Regarding the minimum surface area per molecule, a_s, in Table 1 values for both n = 1 and n = 2 (in parentheses) are shown, as they are limiting values. In principle, n = 1 should be used because of the excess NaOH in solution. This leads to relatively low a_s values for 8Lys8 and 10Lys10, but still plausible for double-chained amphiphiles, considering that the limiting cross-section area of a hydrocarbon chain (solid state) is on the order of 0.20 nm^2. However, for 12Lys12 an unrealistic value of 0.23 nm^2 is obtained, whereas the doubled value (n = 2) might still be not very plausible, as it would imply a rather compact Gibbs monolayer (assuming a limiting value of ca. 0.40 nm^2 for two chains in solid state). Physically meaningless values for molecular surface areas derived from the maximum surface excess of surface tension curves have been reported before, for instance, for DDAB (0.24 nm^2).[52] Thomas et al. have also dealt with the issue of using correct prefactors (n) in Gibbs equation for gemini surfactants, and potential discrepancies between molecular areas derived from surface tension data and those from direct neutron reflectometry.[53] Menger et al. have recently altogether questioned the classical Gibbs analysis of surface adsorption near the cmc, on the basis of NMR diffusivity, conductivity and radiotracer analysis data.[54,55]

In this report, without assessing a_s values of 12Lys12 in Gibbs monolayers by other techniques, we do not dwell more on this issue but rather acknowledge the fact for future investigations (e.g., study of insoluble monolayers). Still, it is possible to infer some qualitative trends in a_s: it decreases with chain length, reflecting the increasing hydrophobicity of the molecules, which promotes strong adsorption at the interface. A similar behavior is seen, for instance, for diakyldimethylammonium surfactants.[52] The existence of groups where intermolecular hydrogen bonding can occur, namely, the N—H and C═O groups, is also expected to enhance the surface adsorption by facilitating the packing of the molecules at the interface.[31,51,56−58]

These lysine-based amphiphiles are aliphatic carboxylates and thus pH influences their solution and aggregation behavior. The apparent pK_a of each surfactant was determined by titration of a 20 mmol·kg^{-1} surfactant solution with hydrochloric acid. The obtained pK_a values were 5.7 for 8Lys8, 8.5 for 10Lys10, and 9.0 for 12Lys12. The increase in the apparent pK_a values is in accordance with the trend observed for *fatty* acid soaps above cmc, for which there is an increase in apparent pK_a with increasing chain length (via an effect of chain length on cmc).[47,59,60] At this concentration all lysine surfactants are above their cmc. The longer chain length makes the soap acids weaker because in the micellar surface it becomes unfavorable to have charges near a low dielectric medium (the micellar core) and because of headgroup repulsions.[59,60]

3.2. Supramolecular Structures at Low Surfactant Concentration: Light and Electron (cryo-SEM) Microscopy Studies. Light microscopy observations on dilute aqueous dispersions of 12Lys12 readily show very interesting features: tubular structures are formed once the samples are cooled from the isotropic solution, inducing gelation of the system. However, no supramolecular aggregation of this type is observed for 8Lys8 and 10Lys10 amphiphiles. To further investigate the structural

dx.doi.org/10.1021/jp400127k | J. Phys. Chem. B 2013, 117, 9400−9411

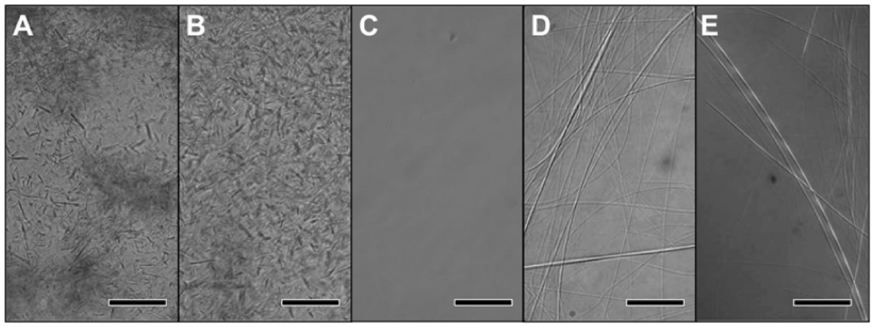

Figure 3. Light micrographs for the solubilization process for a 0.5 wt % 12Lys12 dispersion: (A) 25 °C; (B) 36 °C; (C) 38 °C; (D) 44 °C; (E) 25 °C (perdeuterated D12Lys12 surfactant). Scale bars: 40 μm.

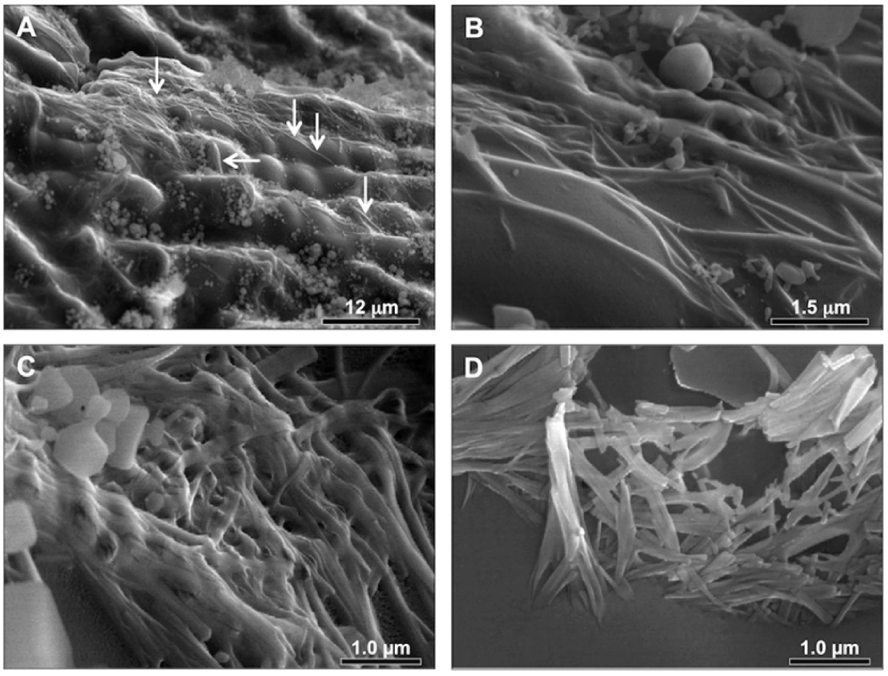

Figure 4. Cryo-SEM imaging of a 0.5 wt % 12Lys12 dispersion. Images belong to two different regions of a unique fracture (A)−(C) and (D). In (A) arrows point to tubules lying on top of the vitrified sample.

features of the 12Lys12 tubules, as well as thermodynamic and kinetic aspects of their self-assembly, microscopy, calorimetric, and solid-state NMR experiments were carried out and will be shown in the next sections. For solid-state NMR, the perdeuterated dodecyl derivative, D12Lys12, was used.

The PLM image sequence presented in Figure 3 shows the solubilization process of 12Lys12 in water and the formation of tubular aggregates, at 0.5 wt % surfactant. At 25 °C, dispersed crystals are observed, with amorphous appearance and without any traces of optical birefringence (Figure 3A). At 36 °C, the crystals undergo a presolubilization process, in which the dispersed crystallites "swell" and become thicker and translucent (Figure 3B). At 38 °C, an increase in the length of these aggregates occurs without further changes. An isotropic solution is obtained at 44 °C (Figure 3C). Cooling the isotropic solution to room temperature induces the formation of tubules (Figure 3D). The solution remains bluish and slightly viscous for a few hours, evolving later and over the next 24h to a white gel-like sample that efficiently traps all the solvent. The tubules are several micrometers long, with some showing ramifications where thinner tubules form. The replacement of protium (^{1}H) by deuterium (^{2}H) in the alkyl chains does not change the ability to form tubules. Interestingly, for the deuterated 12Lys12, tubules and flat tape-like structures are observed with a width of ca. 2−5 μm (Figure 3E).

The cryo-SEM method is particularly useful for the imaging of microstructures of large self-assembled aggregates formed in viscous or concentrated dispersions.[61] Hence, cryo-SEM imaging of preheated 0.5 wt % dispersions was carried out and representative micrographs are shown in Figure 4. Panel A shows an overview of the sample at low magnification, where tubules can be seen lying on top of the vitrified fracture, and panels B−D present magnified structural features. In panel B, one can see that the tubes are fairly cylindrical, with some minor striation on the surface visible for some aggregates. Panels C and D show that ribbons, or tape-like structures, are also present in the same sample. Due to the overcrowding of supramolecular assemblies in this region, some degree of flattening is expected for the hollow cylindrical structures during sample preparation (namely due to shear when the sample holder is filled prior to vitrification). Yet the structures present in panel D appear to be striated tape-like aggregates and not flat tubules. The diameter for the tubules is in the 70−280 nm range and the width for the flat structures is in the 160−400 nm range. Despite the fact that

dx.doi.org/10.1021/jp400127k | J. Phys. Chem. B 2013, 117, 9400−9411

cryo-SEM is susceptible to artifact formation,[61] such as incomplete vitrification and sample deformation by ice crystallization, the tape-like aggregates observed could be reproduced and it is unlikely that they result from artifacts. Moreover, there is some obvious similarity between these structures and those visible in Figure 3E, even accounting for the big difference in scale.

3.3. Tubule Formation by 12Lys12: Effect of Concentration and pH. The formation of tubules by 12Lys12, as a function of concentration (Figures 5 and 6) and pH (Figure 7),

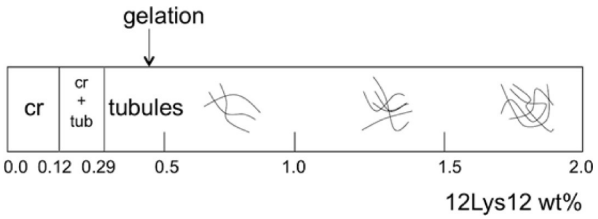

Figure 5. Dilute region phase map of 12Lys12 in water, at θ = 25 °C. Legend: cr, crystals; cr + tub, crystals and tubules. Drawings in the tubule region show the increase in tubule concentration and entanglement with increasing surfactant concentration. The arrow points the concentration (0.4 wt %) where samples gelify.

was further investigated. The schematic phase map in Figure 5 summarizes the main observations for the concentration-dependent behavior (in wt %). The conjugate acid of the 12Lys12 salt is highly insoluble, precipitating out from solution in the form of needle-like crystallites (Figure 6A). Precipitation occurs for samples below 0.29 wt %, a concentration for which the measured pH is 9.0 and thus equal to the apparent pK_a of the surfactant. The formation of needle-shaped acid crystallites is particularly significant below 0.12 wt % (pH <8.2), even at temperatures higher than the Krafft temperature. The formation of soap acid is strongly favored by its insolubility (due to hydrophobicity of the molecule and absence of charge). Precipitation continuously shifts the acid−base equilibrium toward the formation of the acid, eventually depleting all the available carboxylate. The crystallites solubilize, however, if alkali (NaOH) is added to the solution.

In the range 0.12−0.29 wt % (pH = 8.2−9.0), crystals coexist with tubules (Figure 6B). Above 0.29 wt % surfactant, only tubules and no crystallites are observed (similar to what is shown in Figure 6C1). The gelation ability of the samples increases with increasing concentration, and for $c \geq 0.5$ wt %, the gels become extremely strong, resisting flow under vial inversion and remaining stable (without visible solvent separation) for several months, at room temperature. At 0.5 wt %, the initial isotropic solution has pH ≈ 9.4, indicating that once there is a small excess of anionic surfactant, gelification is drastically enhanced. With a further increase in concentration, the density of tubules increases in the gels as well as the degree of entanglement. For $c \geq 1$ wt %, a hexagonal liquid crystalline texture is noticeable through its characteristic birefringent pattern under polarized light (Figure 6C2), becoming more defined with increasing concentration. Below this concentration, just a slight birefringence of the tubular aggregates is observed, mainly in the regions where entanglement occurs. At 2 wt %, a helical configuration is observed for some of the aggregates (Figure 6C1), which becomes a characteristic feature for $c \geq 2$ wt %. These helical structures are presumably intermediate structures in the tubule formation process[32] and will be further discussed in section 3.6.

In fact, the formation of helical aggregates also occurs for more dilute solutions upon a pH increase. Figure 7 shows representative micrographs of aggregates observed for different pH values at 0.5 wt %. If the pH is adjusted below the apparent pK_a, crystallites are formed (Figure 7A, pH = 8.1). When the pH increases, some helical aggregates are observed, with the helix pitch increasing with increasing pH value, as shown in Figure 7B−D (pH = 10−12).

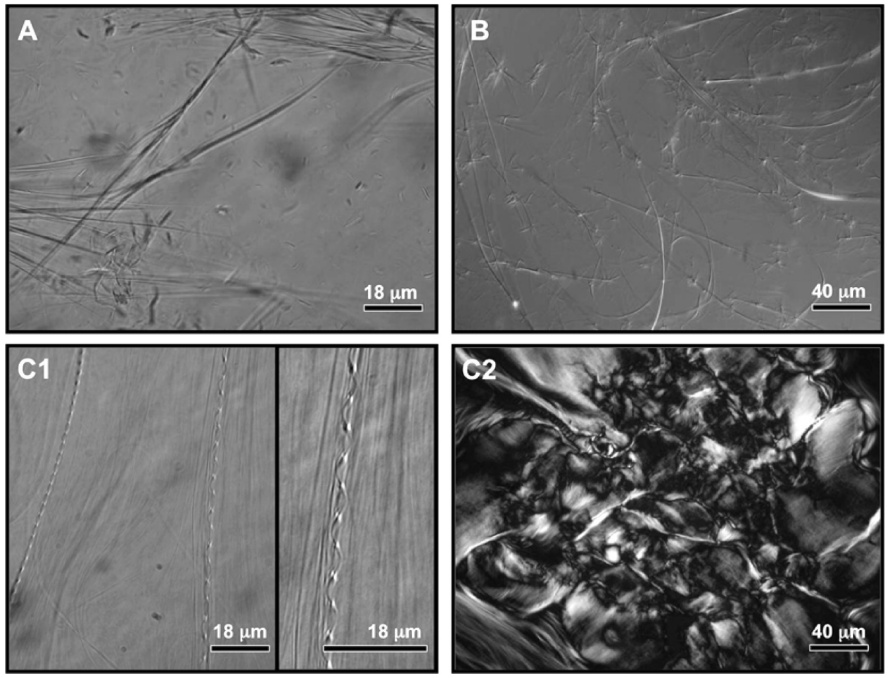

Figure 6. Light micrographs of 12Lys12 dispersions: (A) 0.1 wt %; (B) 0.27 wt %; (C1) and (C2) 2 wt %. (C2) shows the optical texture when the sample is visualized between crossed polarizers. Apparent helix pitch in the inset of C1: 5.1 μm.

dx.doi.org/10.1021/jp400127k | J. Phys. Chem. B 2013, 117, 9400−9411

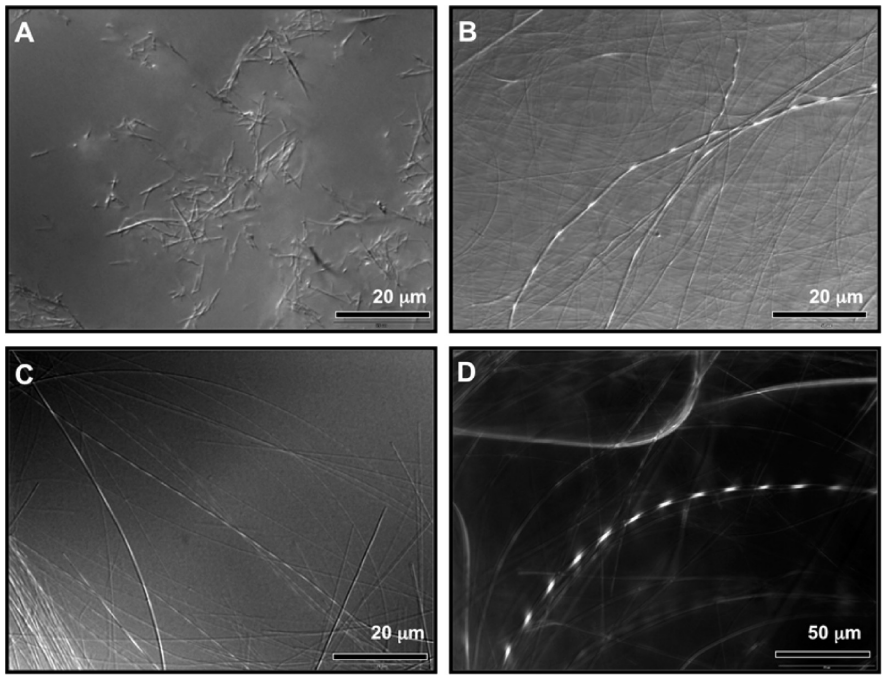

Figure 7. Light micrographs of 12Lys12 tubules under varying pH: (A) pH = 8.1; (B) pH = 10.0; (C) pH = 11.2; (D) pH = 12.1. Apparent helix pitch value: (C) 3.9 μm; (D) 7.5 μm.

3.4. Thermal Behavior of Tubular Structures: Differential Scanning Calorimetry and Solid-State NMR Studies. A detailed calorimetric study of the tubule formation process by 12Lys12 was done. The initial heating scan (Figure 8a), corresponding to the solubilization of crystallites, shows two coalesced endothermic peaks (θ = 38.6 and 40.6 °C), the weakest one at lower temperature, whereas the cooling and reheating scans only exhibit one peak. The phase transition is fully reversible because the solubilization and crystallization enthalpies are equal. Further cooling and reheating scans remain consistent, in both temperature and enthalpy. However, hysteresis is observed with an undercooling of the crystallization of ca. 7 °C.

The first peak in Figure 8a, referred to here as pretransition, disappears if the surfactant crystals are stirred for a long time in water (Figure 8b). Taking into account the microscopy observation that at 38.0 °C the crystals appear to "swell", one can infer that this transition is related to the hydration of the surfactant crystals. A similar phenomenon has been reported for instance in polyglycerol esters.[62] For briefly sonicated, sonicated, and stirred samples, the $\Delta_{trs}H_m$ values associated with the initial heating are roughly the same, 62.0 ± 1.5 kJ·mol^{-1} (Table 2), with an average value per CH_2 group of 2.6 kJ·mol^{-1}, comparable to 1.9−2.1 kJ·mol^{-1} for the solubilization of phospholipids.[63] The only changes observed due to variations in sample preparation concern the solubilization temperatures and the thermogram profile. This hydration phenomenon, once the samples are stirred or temperature-equilibrated (heated until 38.8 °C, cooled and then reheated to 55 °C) is concomitant with chain melting, because the enthalpy values are identical (within the experimental error) for all preparation methods.

Prolonged contact of the crystals results in the absence of the pretransition. Nevertheless, broadening of the single transition is observed and the transition onset temperature does not vary significantly with the preparation procedure. Heating of the samples to 38.8 °C (slightly above the pretransition temperature) and subsequent equilibration for 5 min (temperature equilibration) (Figure 8c), followed by a full heating scan, yields thermogram profiles and thermodynamic parameters similar to those of stirred samples. The solubilization of the crystals is gradual and expected to occur with the simultaneous solubilization of the hydrocarbon chains, as water gradually hydrates the surfactant layers. Above 41.0 °C an isotropic solution forms. Subsequent scans are fully reproducible, with no significant differences between an immediate reheating and a heating scan run two weeks later.

When the behavior of the nondeuterated (Figure 8a) and the deuterated C12 surfactant (Figure 9) are compared, an immediate difference is seen. The latter shows only one broad transition associated with the heating of the solid surfactant crystals dispersed in water, whereas the cooling scan exhibits a two-peak transition. The enthalpies measured for both the heating and cooling scans are comparable in absolute value (Table 3), and hence the phase transition is fully reversible. θ_{trs} and $\Delta_{trs}H_m$ values are slightly lower for the deuterated C12 surfactant.

A study of the kinetics of chain crystallization was also done with the results shown in Figure 10. The differential heat capacity traces are represented by the solid line and the temperature scan (either ramp or isotherm) by the dotted line. After an initial heating with the aim of solubilizing the dispersed crystallites, the samples were cooled to 20.8 °C and kept isothermally at this temperature. The onset of crystallization is much faster for the nondeuterated surfactant than for the deuterated one. For the first, after 50 min the baseline starts to shift, showing an exothermic event, whereas for the deuterated surfactant this only happens after 103 min. Both events take approximately the same time, ca. 70 min. The thermodynamic parameters associated with the experiments are listed in Table 4.

Equilibration at 20.8 °C *per se* is not enough to induce the full crystallization of the D12Lys12 hydrophobic chains. For the nondeuterated surfactant the crystallization is practically

dx.doi.org/10.1021/jp400127k | J. Phys. Chem. B 2013, 117, 9400−9411

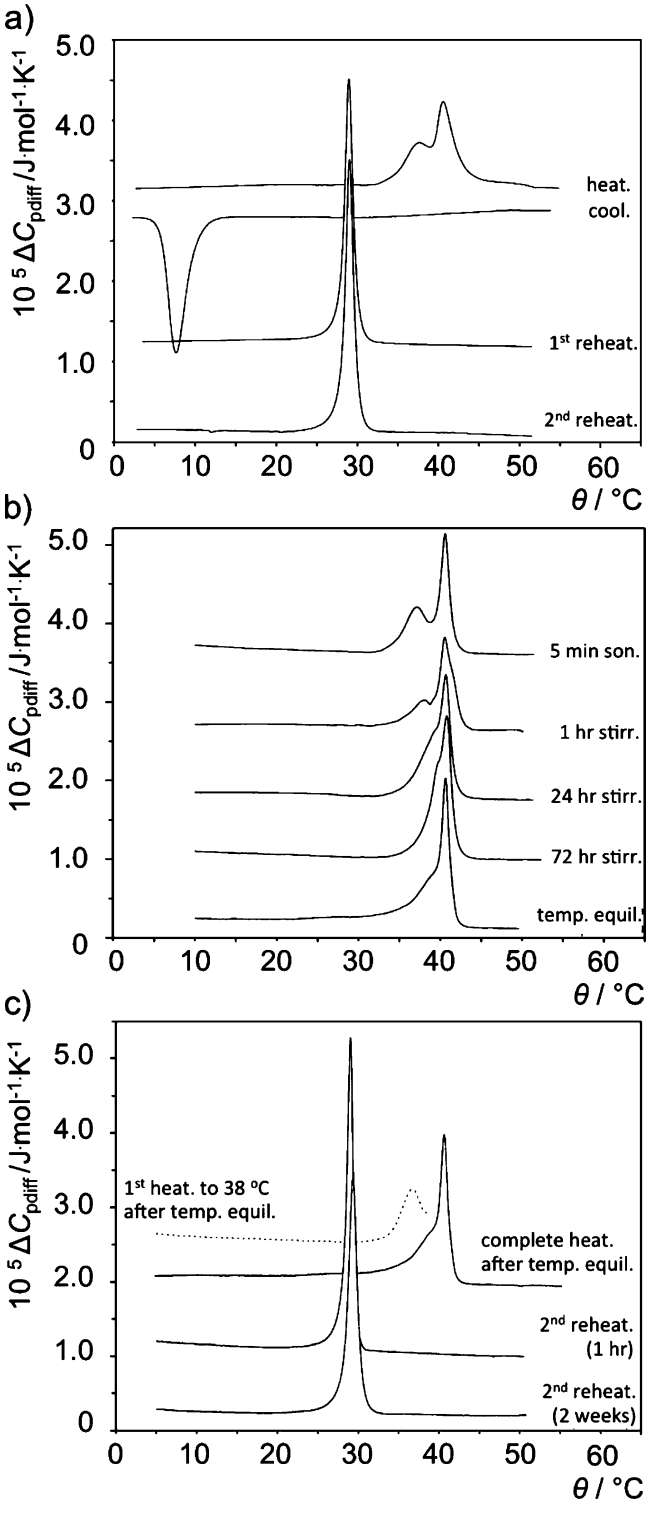

Figure 8. DSC thermograms showing (a) heating−cooling-reheating cycle for a 0.5 wt % 12Lys12 dispersion in water (by sonication), (b) first heating scans after different sample treatments previous to the heating of dispersed crystals, and (c) temperature-equilibrated samples and subsequent reheatings, 1 h and 2 weeks after the initial heating scan. The dotted line indicates the temperature-equilibration cycle.

complete, as 90% of the transition enthalpy is recovered. In contrast, the deuterated surfactant does not recover completely the crystalline state, as there is a 40% difference between the initial solubilization and the isothermal crystallization. This clearly indicates an incomplete crystallization of the system. For

Table 2. Thermodynamic Parameters (Temperature, θ_{trs}; Transition Molar Enthalpy, $\Delta_{trs}H_m$; Transition Molar Entropy, $\Delta_{trs}S_m$) for Solubilization and Recrystallization of 12Lys12 Tubules (0.5 wt %) in Water, As Obtained from DSC[a]

sample prepn method	scan	$\theta_{trs,on}$[b]/°C	$\theta_{trs,peak}$[c]/°C	$\Delta_{trs}H_m$/kJ·mol^{-1}	$\Delta_{trs}S_m$/J·K^{-1}·mol^{-1}
brief sonication	heating	32.3	38.6	60.7	193.5
			40.6		
	cooling	14.7	7.6	−60.8	−216.6
	1st reheating	22.5	28.9	62.5	206.9
	2nd reheating	22.1	29.0	63.3	209.5
5 min sonication	heating	30.9	37.1	63.2	201.4
			40.6		
1h stirring	heating	31.4	38.1	59.2	188.7
			40.5		
24h stirring	heating	32.2	40.7	62.2	198.2
72h stirring	heating	34.1	40.8	63.1	201.0
temperature-equilibration (to 38 °C)	partial heating	30.7	36.7		
temperature-equilibration (full scan)	complete heating	22.0	40.6	69.9	222.8
1 h aging	1st reheating	23.3	29.0	65.7	217.4
2 weeks aging	2nd reheating	24.2	29.4	66.3	219.1

[a]Typical uncertainty values: ±0.3 °C for temperatures; ±5% for both $\Delta_{trs}H_m$ and $\Delta_{trs}S_m$. [b]Onset temperature of phase transition. [c]Temperature at peak maximum.

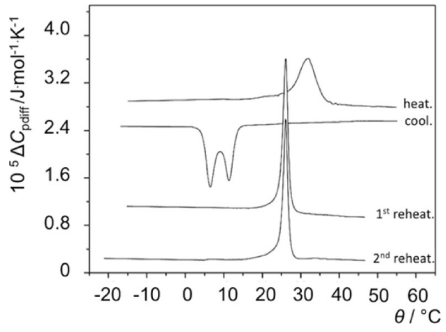

Figure 9. DSC thermograms with heating−cooling−reheating cycles for a 0.5 wt % D12Lys12 dispersion in water.

Table 3. Thermodynamic Parameters (Temperature, θ_{trs}; Transition Molar Enthalpy, $\Delta_{trs}H_m$; Transition Molar Entropy, $\Delta_{trs}S_m$) for Solubilization and Recrystallization of D12Lys12 (Perdeuterated Surfactant) Tubules (0.5 wt %) in Water, As Obtained from DSC[a]

scan	$\theta_{trs,on}$[b]/°C	$\theta_{trs,peak}$[c]/°C	$\Delta_{trs}H_m$/kJ·mol^{-1}	$\Delta_{trs}S_m$/J·K^{-1}·mol^{-1}
heating	17.5	32.0	56.0	183.5
cooling	15.7	6.4, 11.4	−62.8	−220.7
1st reheating	18.6	26.1	58.3	194.8
2nd reheating	17.2	26.1	57.9	193.5

[a]Typical uncertainty values: ±0.3 °C for temperatures; ±5% for both $\Delta_{trs}H_m$ and $\Delta_{trs}S_m$. [b]Onset temperature of phase transition. [c]Temperature of peak maximum.

dx.doi.org/10.1021/jp400127k | J. Phys. Chem. B 2013, 117, 9400−9411

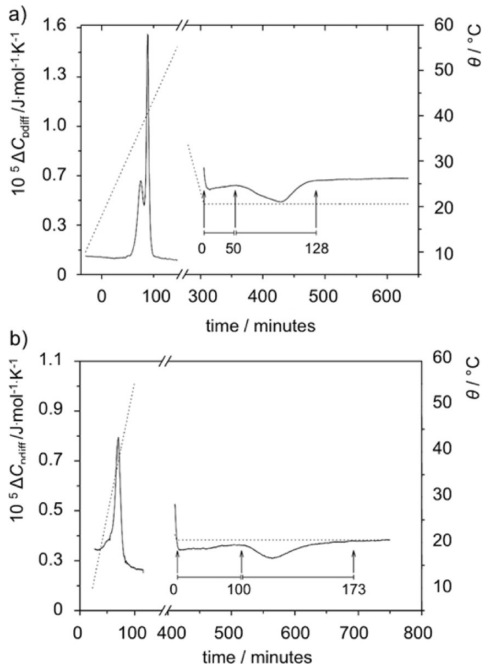

Figure 10. DSC thermogram of the crystallization process as a function of time for a 0.5 wt % tubule dispersion of (a) 12Lys12 and (b) D12Lys12. The black line represents differential heat capacity traces and dashed line shows the temperature ramp.

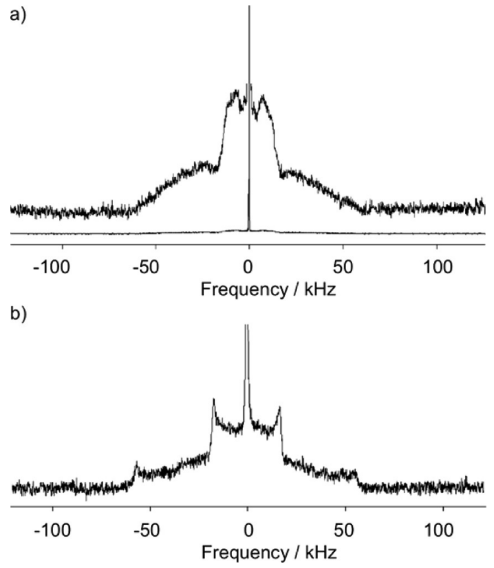

Figure 11. (a) Deuterium NMR spectrum of a 1.5% dispersion of the 12Lys12 solid in water at room temperature. The whole spectrum is shown to better visualize the contribution of the isotropic line and an enlargement is also shown illustrating the shape of the powder patterns. (b) Deuterium NMR spectrum of a 1.5% dispersion of 12Lys12 tubules in water at room temperature after heating and cooling the dispersion. The top of isotropic peak was truncated to better visualize the change in the powder pattern shape.

the solid-state NMR studies, the sample was cooled below 6 °C, where crystallization is complete.

Solid-state NMR was then used to check the state of the hydrophobic chains in the tubular aggregates and in the isotropic phase formed after the solubilization. At room temperature, the NMR spectrum is basically composed of the superimposition of two main broad powder patterns together with an isotropic line (Figure 11a). The width of the powder patterns is more or less typical of surfactants embedded in a hydrated crystalline phase with a large asymmetry parameter. The smallest spectrum with a splitting of less than 40 kHz corresponds to methyl groups[64,65] whereas the largest one corresponds to the methylene groups. When the sample is heated, the spectrum turns to a unique isotropic peak at 32 °C, suggesting that the tubules have melted and given rise to an isotropic (micellar) solution. This is a common feature for such supramolecular assemblies.[34,66] After the sample cools (Figure 10b), the isotropic line remains, showing that metastable isotropic aggregates could still be present. The main feature, though, is that the powder patterns now exhibit a shape without asymmetry parameters and are better resolved. One can clearly assign the terminal methyl groups having a splitting of 37 kHz and the methylene groups having a splitting of 125 kHz. These values are typical of alkyl chains embedded in a crystalline phase, i.e., chains that are fully stretched.

3.5. Concentrated Surfactant–Water Systems: Phase Scanning Studies. To further determine the self-assembly features for the lysine-based amphiphiles, phase scans were carried out in the polarized light microscope. Observations were performed at 25.0 °C except for the 12Lys12 amphiphile (50.0 °C), because this amphiphile is not soluble at room temperature. The 8Lys8 amphiphile (Figure 12A) shows a dilute isotropic L_1 phase, followed by two different textures: a lower concentration striated texture, indicating a hexagonal phase (H_1), and a higher concentration mosaic texture, corresponding to a lamellar phase (L_α). The 10Lys10 amphiphile also shows an interesting behavior. Here the phase boundaries appear to be clearer and the textures more defined than in the previous surfactant. A dilute L_1 phase is present, where the acid–base equilibrium allows the formation of the needle-like crystals (Figure 12B). With increasing concentration, a hexagonal phase forms, followed by a lamellar phase (Grandjean steps texture), before the hydrated crystals are reached.

Table 4. Thermodynamic Parameters (Temperature, θ_{trs}; Transition Molar Enthalpy, $\Delta_{trs}H_m$; Transition Molar Entropy, $\Delta_{trs}S_m$) for Solubilization and Crystallization Kinetics (Δt_{on}, Time Lag for Onset of Crystallization; Δt_{trs}, Time Length of Crystallization Process) for 0.5 wt % Tubule Dispersions of Nondeuterated 12Lys12 (H) and Perdeuterated 12Lys12 (D) in Water[a]

	$\theta_{trs,on}$[b]/°C		$\theta_{trs,peak}$[c]/°C		$\Delta_{trs}H_m$/kJ·mol^{-1}		$\Delta_{trs}S_m$/J·K^{-1}·mol^{-1}		Δt_{on}/min		Δt_{trs}/min	
cycle	H	D	H	D	H	D	H	D	H	D	H	D
initial heating	29.4	11.7	37.3 40.5	26.2	65.2	59.7	207.9	199.4				
isotherm (θ = 20.6 °C)					59.1	34.1	201.2	−116.1	50	103	78	173

[a]Typical uncertainty values: ±0.3 °C for temperatures; ±5% for both $\Delta_{trs}H_m$ and $\Delta_{trs}S_m$. [b]Onset temperature of phase transition. [c]Temperature of peak maximum.

dx.doi.org/10.1021/jp400127k | J. Phys. Chem. B 2013, 117, 9400–9411

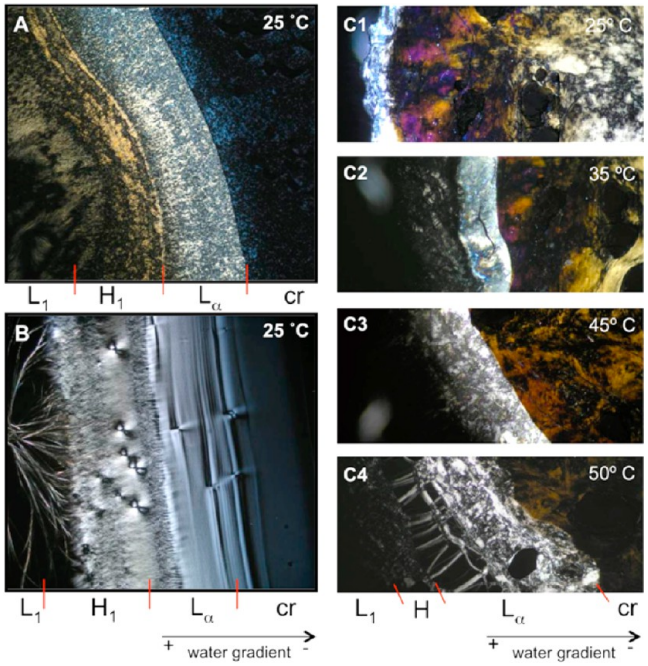

Figure 12. Phase penetration scans: (A) 8Lys8, at 25 °C; (B) 10Lys10, at 25 °C (C1−C4) 12Lys12, at the indicated temperatures. Legend: L_1, micellar phase; H, hexagonal phase; L_α, lamellar phase; cr, hydrated crystals. Water is diffusing from left to right into the surfactant crystalline film.

The 12Lys12 phase scans were done upon heating of the sample and the results are shown in Figure 12C1−4. At 25.0 °C, hydration of the surfactant crystallites is poor and only small birefringent domains are visibly formed (Figure 12C1). With increasing temperature (35 °C, Figure 12C2), water diffuses into the solid, forming an undefined texture. At 45.0 °C, an isotropic L_1 phase forms together with a mosaic texture at higher concentration, indicating presence of L_α (Figure 12C3). The presence of a hexagonal phase (nongeometric, striated texture) between L_1 and L_α is only clearly visible at 50.0 °C (Figure C4). The lamellar phase is also now apparent in the form of oily streaks followed by the mosaic texture at higher concentration.

In summary, once the surfactant is fully hydrated and with liquid-like chains, the molecules follow a common phase sequence (micellar solution → hexagonal phase → lamellar phase, Table 5), which is more typical for single-chained than for double-chained surfactants. For a conventional double-chained amphiphile, like dialkyldimethylammonium halides or phospholipids, the phase behavior would be dominated by a lamellar phase (as the single liquid crystalline phase) and dispersions of vesicular structures at low concentration.[29,51,52] One possible reason for the nLysn behavior is that the gemini-like configuration in the fluid surfactant film is slightly distorted around the spacer region. The two alkyl chains may bend and approach each other, in such a way that a cone-shaped geometry is attained rather than a cylindrical one. This would imply a critical packing parameter (P_s) value sufficiently low to allow for micelle formation (albeit nonspherical), $P_s < 1/2$, rather than one that could be expected for a double-chained amphiphile ($P_s \approx 1$).

3.6. Rationalization of Supramolecular Aggregation. A global analysis of the experimental data allows for a qualitative rationalization of the tubule assembly process for 12Lys12. The initial solubilization of the crystals seems to begin with the hydration of the headgroup layers, which is an irreversible process, because all scans subsequent to the first do not show a pretransition (as illustrated by Figure 8a, at 0.5 wt %). This temperature is ca. 10 °C below the chain melting process of the hydrated crystals. Chain recrystallization is a relatively slow process (hours) if samples are allowed to equilibrate at room temperature. Reheating induces now a phase transition (essentially chain melting) of surfactant already self-assembled in tubular aggregates. The tubule melting appears to be highly cooperative, suggesting that no intermediate bilayer gel phase exists between the tubules and the isotropic phase,[67] which consists of a micellar solution.

Light micrographs of concentrated samples of 12Lys12 ($c >$ 0.5 wt %) show the presence of helically coiled aggregates (Figure 6C1). These aggregates are expected to appear during the process of tubule formation. If this process occurs via a helical intermediate (the common case when the surfactant has a chiral headgroup), it usually follows one of two paths. One involves the shortening of the helix pitch, maintaining constant the helix tape width, whereas in the second path widening of the helix tape width occurs, while the helix pitch is kept constant (Figure 13).[21,68] Although it was not possible to distinguish between these two mechanisms in this work, the coiled aggregates are thought to be related to tubule formation upon cooling of the isotropic solution. One possible reason for the visualization of the intermediate helix for the more concentrated samples is the crowding effect induced by the larger volume fraction of surfactant in the system. It can be pictured that the conversion from helices to tubules will be "slower" (concentration-wise) as the available volume for the latter is smaller, slowing down even more as more tubules are formed. Once the temperature decreases and the chains crystallize, helices may get kinetically trapped due to the overall slowdown of the system dynamics.

The formation of intermediate helical structure suggests that not only hydrophobic interactions and hydrogen bonding are driving the tubule assembly but also chirality. This implies that tubule formation follows a chirality-induced mechanism, in which each monolayer is a mirror image of the adjacent one.[37,67]

Table 5. Phase Sequence for the Lysine-Based Surfactants, with Typical Textures Observed under Polarized Light Listed below the Corresponding Liquid-Crystalline Phase[a]

surfactant	phase sequence						
8Lys8	L_1	→	H_I	→	L_α	→	cr
	isotropic		striated texture		mosaic texture		
10Lys10	L_1	→	H_I	→	L_α	→	cr
	isotropic		striated texture		Grandjean steps		
12Lys12	L_1	→	H_I	→	L_α	→	cr
	isotropic		striated texture		oily streaks		

[a]Legend: L_1, micellar phase; H, hexagonal phase; L_α, lamellar phase; cr, hydrated crystals.

dx.doi.org/10.1021/jp400127k | J. Phys. Chem. B 2013, 117, 9400−9411

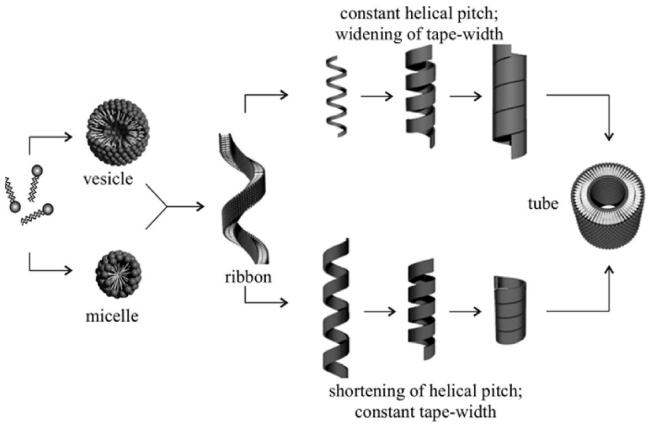

Figure 13. Mechanisms of tubule formation by the chirality-dependent process: widening of the tape width with constant helix pitch or shortening of the helix pitch keeping constant the helix tape width (adapted from ref 4).

A small tilting of the molecular axis would occur between adjacent molecules, favoring the wrapping of the bilayers into tubular aggregates. Because the bilayers are mirror images of one another, the tilt angles are symmetric and the two monolayers acquire also symmetric spontaneous curvature values. Thus, the inner and outer monolayer curvature problem in the assembly process is overcome. Highly stable aggregates should be formed, mainly due to the highly ordered packing of the molecules.

Electrostatic interactions also play an active role in the formation and structure of the tubular aggregates through the soap/acid concentration ratio, $r = |RCOO^-|/|RCOOH|$. Below 0.29 wt % surfactant (pH = 9.0), $r \leq 1$ and crystals coexist with tubules. This means tubules are only formed when the surfactant layers possess some critical surface charge density. Repulsive electrostatic interactions stabilize the tubular aggregates by counteracting the attractive van der Waals forces that would collapse the system. Once $r > 1$, only tubules are observed, but with a morphology that is dependent on concentration and pH. For 2 wt % (Figure 6C2) helically twisted tubules are seen at natural pH, just as for 0.5 wt % under pH increase, suggesting that higher r (and thus higher charge density in the bilayers) should promote helical twisting. Nevertheless, it is not clear if these are metastable or equilibrium structures; this issue was not fully addressed in this work, and will be subject to further investigations.

Tubule formation is not observed for the shorter chain C8 and C10 surfactants. Here, hydrophobic interactions are weaker than in 12Lys12 and thus not strong enough to stabilize tubular aggregates when the chains crystallize. It is possible that a critical chain length of C12 is necessary and in fact the same effect has been observed for other tubule-forming systems.[12,22] This observation also confirms that solvent gelation by amphiphilic molecules results from the balance between hydrogen bonding and hydrophobicity of the molecule, allowing the formation of a strongly cohesive 3D network. Hydrogen bonding between the secondary amide and the carboxylate groups, together with the chiral effect, assists molecular assembly into a highly organized array. This increases the contact between hydrophobic chains, increasing the magnitude of van der Waals interactions. Above the chain melting temperature, thermal agitation of the fluid chains and concomitant changes in the P_s value disrupt both the short-range and long-range order. Weakening of hydrophobic interactions, together with the change of the most favorable curvature, presumably dictates the formation of micelles above the tubule melting temperature.

4. CONCLUSION

In this work, we have investigated the interfacial and self-assembling properties of double-chained lysine-based amphiphiles. These compounds are strongly surface-active micelle-forming amphiphiles. As shown from microscopy data, the 12Lys12 derivative forms tubules upon cooling from an isotropic micellar solution, whereas the shorter chain homologues do not. DSC and NMR studies show that formation of tubules implies chain crystallization. The integrity and overall rigidity of the tubules is presumed to be due to hydrogen bonding between the polar headgroups and hydrophobic interactions. The ordered packing of the molecules in the tubular architecture per se should be due to the existence of a chiral center in the surfactant headgroug. Electrostatic interactions seem also to play an important role in self-assembly, as evidenced from pH variation studies. Tubules do not form at lower pH values, when a high fraction of surfactant is in neutral acidic form.

An overview of the phase behavior of the lysine-based amphiphiles has also been presented by phase scan microscopy. With increasing concentration, the following phase sequence is observed: micellar phase−hexagonal phase−lamellar phase−hydrated crystals. This sequence is in agreement with what is expected for surfactants with a packing parameter in the range 1/3−1/2 rather than one for conventional double-chained amphiphile (which would form bilayers structures throughout). In turn, this implies that the nLysn molecules, once the chains are in molten state, tend to adopt an overall cone-shaped configuration rather than a cylindrical one.

AUTHOR INFORMATION

Corresponding Author

*E-mail: efmarque@fc.up.pt. Tel.: +351 22 0402 535 Fax: +351 22 0402 659.

Notes

The authors declare no competing financial interest.

ACKNOWLEDGMENTS

We are greatly indebted to Dr. Jean-Paul Douliez (I.N.R.A., Nantes) for the ^{2}H NMR experiments and for interesting discussions throughout this work. The authors kindly acknowledge financing from FEDER through Programa COMPETE and national funding through FCT, Fundação para a Ciência e Tecnologia, under projects PEST-C/QUI/UI0081/2011 and PTDC/QUI-QUI/115212/2009.

REFERENCES

(1) Holmberg, K. Natural Surfactants. *Curr. Opin. Colloid Interface Sci.* **2001**, *6*, 148−159.

(2) Szuts, A.; Szabo-Revesz, P. Sucrose Esters as Natural Surfactants in Drug Delivery Systems-a Mini-Review. *Int. J. Pharm.* **2012**, *433*, 1−9.

(3) Hill, K. Fats and Oils as Oleochemical Raw Materials. *Pure Appl. Chem.* **2000**, *72*, 1255−1264.

(4) Shimizu, T.; Masuda, M.; Minamikawa, H. Supramolecular Nanotube Architectures Based on Amphiphilic Molecules. *Chem. Rev.* **2005**, *105*, 1401−1444.

(5) Sánchez, L.; Mitjans, M.; Infante, M. R.; García, M. T.; Manresa, M. A.; Vinardell, M. P. The Biological Properties of Lysine-Derived Surfactants. *Amino Acids* **2007**, *32*, 133−136.

(6) Pinazo, A.; Pons, R.; Perez, L.; Infante, M. R. Amino Acids as Raw Material for Biocompatible Surfactants. *Ind. Eng. Chem. Res.* **2011**, *50*, 4805−4817.
(7) Takahashi, R.; Ishiwatari, T. Preparation of Helical Gold Nanowires on Surfactant Tubules. *Chem. Commun.* **2004**, *12*, 1406−1407.
(8) Mitra, A.; Imae, T.; Shchipunov, Y. A. Fibrous Silica Composites Fabricated Via Sol−Gel Processing Using Amino Acid Surfactant Templating. *J. Sol-Gel Sci. Technol.* **2005**, *34*, 127−130.
(9) Sen, J.; Chaudhuri, A. Gene Transfer Efficacies of Novel Cationic Amphiphiles with Alanine, b-Alanine, and Serine Headgroups: A Structure-Activity Investigation. *Bioconjugate Chem.* **2005**, *16*, 903−912.
(10) Rosa, M.; Infante, M. R.; Miguel, M. D.; Lindman, B. Spontaneous Formation of Vesicles and Dispersed Cubic and Hexagonal Particles in Amino Acid-Based Catanionic Surfactant Systems. *Langmuir* **2006**, *22*, 5588−5596.
(11) Marques, E. F.; Brito, R. O.; Silva, S. G.; Vale, M. L.; Gomes, P.; Araújo, M. J.; Söderman, O. Spontaneous Vesicle Formation in Catanionic Mixtures of Amino Acid-Based Surfactants: Chain Length Symmetry Effects. *Langmuir* **2008**, *24*, 11009−11017.
(12) Gonzalez, Y. I.; Kaler, E. W. Fibrous Assemblies and Water Gelation in Mixtures of Lysine with Sodium Alkyl Sulfates. *Langmuir* **2005**, *21*, 7191−7199.
(13) Estroff, L. A.; Hamilton, A. D. Water Gelation by Small Organic Molecules. *Chem. Rev.* **2004**, *104*, 1201−1217.
(14) Lee, J. H.; Gustin, J. P.; Chen, T.; Payne, G. F.; Raghavan, S. R. Vesicle-Biopolymer Gels: Networks of Surfactant Vesicles Connected by Associating Biopolymers. *Langmuir* **2005**, *21*, 26−33.
(15) Infante, M. R.; Perez, L.; Pinazo, A.; Clapes, P.; Moran, M. C.; Angelet, M.; Garcia, M. T.; Vinardell, M. P. Amino Acid-Based Surfactants. *C. R. Chim.* **2004**, *7*, 583−592.
(16) Brito, R. O.; Marques, E. F.; Silva, S. G.; Vale, M. L. d.; Gomes, P.; Araújo, M. J.; Rodriguez-Borges, J. E.; Infante, M. R.; Garcia, M. T.; Ribosa, I.; Vinardell, M. P.; Mitjans, M. Physicochemical and Toxicological Properties of Novel Amino Acid-Based Amphiphiles and Their Spontaneously Formed Catanionic Vesicles. *Colloids Surf. B: Biointerfaces* **2009**, *72*, 80−87.
(17) Pérez, N.; Pérez, L.; Infante, M. R.; García, M. T. Biological Properties of Arginine-Based Glycerolipidic Cationic Surfactants. *Green Chem.* **2005**, *7*, 540−546.
(18) Roy, S.; Das, P. K. Antibacterial Hydrogels of Amino Acid-Based Cationic Amphiphiles. *Biotechnol. Bioeng.* **2008**, *100*, 756−764.
(19) Sanchez, L.; Mitjans, M.; Infante, M. R.; Vinardell, M. P. Potential Irritation of Lysine Derivative Surfactants by Hemolysis and Hacat Cell Viability. *Toxicol. Lett.* **2006**, *161*, 53−60.
(20) Silva, S. G.; Alves, C.; Cardoso, A. M. S.; Jurado, A. S.; de Lima, M. C. P.; Vale, M. L. C.; Marques, E. F. Synthesis of Gemini Surfactants and Evaluation of Their Interfacial and Cytotoxic Properties: Exploring the Multifunctionality of Serine as Headgroup. *Eur. J. Org. Chem.* **2013**, 1758−1769.
(21) Chung, D. S.; Benedek, G. B.; Konikoff, F. M.; Donovan, J. M. Elastic Free Energy of Anisotropic Helical Ribbons as Metastable Intermediates in the Crystallization of Cholesterol. *Proc. Natl. Acad. Sci. U. S. A.* **1993**, *90*, 11341−11345.
(22) Roy, S.; Dasgupta, A.; Das, P. K. Alkyl Chain Length Dependent Hydrogelation of L-Tryptophan-Based Amphiphile. *Langmuir* **2007**, *23*, 11769−11776.
(23) Mohanty, A.; Dey, J. Effect of the Headgroup Structure on the Aggregation Behavior and Stability of Self-Assemblies of Sodium N-[4-(n-Dodecyloxy)benzoyl]-L-aminoacidates in Water. *Langmuir* **2007**, *23*, 1033−1040.
(24) Zarif, L. Elongated Supramolecular Assemblies in Drug Delivery. *J. Controlled Release* **2002**, *81*, 7−23.
(25) Zhao, Y.-X.; Shaw, A.; Zeng, X.; Benson, E.; Nystrom, A. M.; Hogberg, B. DNA Origami Delivery System for Cancer Therapy with Tunable Release Properties. *ACS Nano* **2012**, *6*, 8684−8691.
(26) He, J.; Liu, Y.; Babu, T.; Wei, Z.; Nie, Z. Self-Assembly of Inorganic Nanoparticle Vesicles and Tubules Driven by Tethered Linear Block Copolymers. *J. Am. Chem. Soc.* **2012**, *134*, 11342−11345.
(27) Xie, Y.; Zhou, L.; Huang, H. Bioelectrocatalytic Application of Titania Nanotube Array for Molecule Detection. *Biosens. Bioelectron.* **2007**, *22*, 2812−2818.
(28) Ringler, P.; Muller, W.; Ringsdorf, H.; Brisson, A. Functionalized Lipid Tubules as Tools for Helical Crystallization of Proteins. *Chem.—Eur. J.* **1997**, *3*, 620−625.
(29) Antunes, F. E.; Marques, E. F.; Lindman, B.; Miguel, M. Polymer-Vesicle Association. *Adv. Colloid Interface Sci.* **2009**, *147−148*, 18−35.
(30) Oda, R.; Artzner, F.; Laguerre, M.; Huc, I. Molecular Structure of Self-Assembled Chiral Nanoribbons and Nanotubules Revealed in the Hydrated State. *J. Am. Chem. Soc.* **2008**, *130*, 14705−14712.
(31) Brito, R. O.; Marques, E. F.; Gomes, P.; Falcão, S.; Söderman, O. Self-Assembly in a Catanionic Mixture with an Aminoacid-Derived Surfactant: From Mixed Micelles to Spontaneous Vesicles. *J. Phys. Chem. B* **2006**, *110*, 18158−18165.
(32) Shao, H.; Gao, M.; Kim, S. H.; Jaroniec, C. P.; Parquette, J. R. Aqueous Self-Assembly of L-Lysine-Based Amphiphiles into 1D n-Type Nanotubes. *Chem.—Eur. J.* **2011**, *17*, 12882−12885.
(33) Kiagus-Armad, R.; Brizard, A.; Tang, C.; Blatchly, R.; Desbat, B.; Oda, R. Cooperative and Reciprocal Chiral Structure Formation of an Alanine-Based Peptide Confined at the Surface of Cationic Surfactant Membranes. *Chem.—Eur. J.* **2011**, *17*, 9999−10009.
(34) Douliez, J.-P.; Gaillard, C.; Navailles, L.; Nallet, F. Novel Lipid System Forming Hollow Microtubes at High Yields and Concentration. *Langmuir* **2006**, *22*, 2942−2945.
(35) Meijide, F.; Antelo, A.; Alcalde, M. A.; Jover, A.; Galantini, L.; Pavel, N. V.; Tato, J. V. Supramolecular Structures Generated by a p-tert-Butylphenylamide Derivative of Deoxycholic Acid. From Planar Sheets to Tubular Structures through Helical Ribbons. *Langmuir* **2010**, *26*, 7768−7773.
(36) Zhai, L.; Herzog, B.; Drechsler, M.; Hoffmann, H. Novel Nanotubes from a Cationic Surfactant and an Anionic Stiff Aromatic Counter-Ion. *J. Phys. Chem. B* **2006**, *110*, 17697−17701.
(37) Spector, M. S.; Selinger, J. V.; Singh, A.; Rodriguez, J. M.; Price, R. R.; Schnur, J. M. Controlling the Morphology of Chiral Lipid Tubules. *Langmuir* **1998**, *14*, 3493−3500.
(38) Thomas, B. N.; Lindemann, C. M.; Corcoran, R. C.; Cotant, C. L.; Kirsch, J. E.; Persichini, P. J. Phosphonate Lipid Tubules II. *J. Am. Chem. Soc.* **2002**, *124*, 1227−1233.
(39) Imae, T.; Funayama, K.; Krafft, M. P.; Giulieri, F.; Tada, T.; Matsumoto, T. Small-Angle Scattering and Electron Microscopy Investigation of Nanotubules Made from a Perfluoroalkylated Glucophospholipid. *J. Colloid Interface Sci.* **1999**, *212*, 330−337.
(40) Kulkarni, V. S.; Boggs, J. M.; Brown, R. E. Modulation of Nanotube Formation by Structural Modifications of Sphingolipids. *Biophys. J.* **1999**, *77*, 319−330.
(41) Meijide, F.; Trillo, J. V.; Frutos, S. d.; Galantini, L.; Pavel, N. V.; Soto, V. H.; Jover, A.; Tato, J. V. Formation of Tubules by p-tert-Butylphenylamide Derivatives of Chenodeoxycholic and Ursodeoxycholic Acids in Aqueous Solution. *Steroids* **2012**, *77*, 1205−1211.
(42) Ihara, H.; Takafuji, M.; Hirayama, C.; O'Brien, D. F. Effect of Photopolymerization on the Morphology of Helical Supramolecular Assemblies. *Langmuir* **1992**, *8*, 1548−1553.
(43) Yu, K.; Eisenberg, A. Bilayer Morphologies of Self-Assembled Crew-Cut Aggregates of Amphiphilic PS-b-PEO Diblock Copolymers in Solution. *Macromolecules* **1998**, *31*, 3509−3518.
(44) Brito, R. O.; Marques, E. F.; Gomes, P.; Araujo, M. J.; Pons, R. Structure/Property Relationships for the Thermotropic Behavior of Lysine-Based Amphiphiles: from Hexagonal to Smectic Phases. *J. Phys. Chem. B* **2008**, *112*, 14877−14887.
(45) Colomer, A.; Pinazo, A.; Manresa, M. A.; Vinardell, M. P.; Mitjans, M.; Infante, M. R.; Pérez, L. Cationic Surfactants Derived from Lysine: Effects of Their Structure and Charge Type on Antimicrobial and Hemolytic Activities. *J. Med. Chem.* **2011**, *54*, 989−1002.
(46) Colomer, A.; Pinazo, A.; García, M. T.; Mitjans, M.; Vinardell, M. P.; Infante, M. R.; Martínez, V.; Pérez, L. pH-Sensitive Surfactants from Lysine: Assessment of Their Cytotoxicity and Environmental Behavior. *Langmuir* **2012**, *28*, 5900−5912.

(47) Mezei, A.; Pérez, L.; Pinazo, A.; Comelles, F.; Infante, M. R.; Pons, R. Self Assembly of pH-Sensitive Cationic Lysine Based Surfactants. *Langmuir* **2012**, *28*, 16761−16771.
(48) Gomes, P.; Araújo, M. J.; Marques, E. F.; Falcão, S.; Brito, R. O. A Straightforward Method for the Preparation of Lysine-Based Double-Chained Anionic Surfactants. *Synth. Commun.* **2008**, *38*, 2013−2024.
(49) Zana, R. Dimeric and Oligomeric Surfactants. Behavior at Interfaces and in Aqueous Solution: A Review. *Adv. Colloid Interface Sci.* **2002**, *97*, 205−253.
(50) Merta, J.; Garamus, V. M.; Kuklin, A. I.; Willumeit, R.; Stenius, P. Determination of the Structure of Complexes Formed by a Cationic Polymer and Mixed Anionic Surfactants by Small-Angle Neutron Scattering. *Langmuir* **2000**, *16*, 10061−10068.
(51) Jönsson, B.; Lindman, B.; Holmberg, K.; Kronberg, B. *Surfactants and Polymers in Aqueous Solution*; John Wiley & Sons: New York, 1998.
(52) Svitova, T. F.; Smirnova, Y. P.; Pisarev, S. A.; Berezina, N. A. Self-Assembly in Double-Tailed Surfactants in Dilute Aqueous Solutions. *Colloids Surf., A* **1995**, *98*, 107−115.
(53) Li, P. X.; Dong, C. C.; Thomas, R. K.; Penfold, J.; Wang, Y. Neutron Reflectometry of Quaternary Gemini Surfactants as a Function of Alkyl Chain Length: Anomalies Arising from Ion Association and Premicellar Aggregation. *Langmuir* **2011**, *27*, 2575−2586.
(54) Menger, F. M.; Shi, L.; A., R. S. A. Re-evaluating the Gibbs Analysis of Surface Tension at the Air/Water Interface. *J. Am. Chem. Soc.* **2009**, *131*, 10380−10381.
(55) Menger, F. M.; Rizvi, S. A. A. Relationship between Surface Tension and Surface Coverage. *Langmuir* **2011**, *27*, 13975−13977.
(56) Fuhrhop, J. H.; Schnieder, P.; Rosenberg, J.; Boekema, E. The Chiral Bilayer Effect Stabilizes Micellar Fibers. *J. Am. Chem. Soc.* **1987**, *109*, 3387−3390.
(57) Imae, T.; Takahashi, Y.; Muramatsu, H. Formation of Fibrous Molecular Assemblies by Amino Acid Surfactants in Water. *J. Am. Chem. Soc.* **1992**, *115*, 3414−3419.
(58) Boettcher, C.; Schade, B.; Fuhrhop, J. H. Comparative Cryo-Electron Microscopy of Noncovalent N-Dodecanoyl- (D- and L-) Serine Assemblies in Vitreous Toluene and Water. *Langmuir* **2001**, *17*, 873−877.
(59) Goldsipe, A.; Blankschtein, D. Molecular-Thermodynamic Theory of Micellization of pH-Sensitive Surfactants. *Langmuir* **2006**, *22*, 3547−3559.
(60) Söderman, O.; Jönsson, B.; Olofsson, G. Titration of Fatty Acids Solubilized in Cationic and Anionic Micelles. Calorimetry and Thermodynamic Modeling. *J. Phys. Chem. B* **2006**, *110*, 3288−3293.
(61) Issman, L.; Talmon, Y. Cryo-SEM Specimen Preparation under Controlled Temperature and Concentration Conditions. *J. Microsc. (Paris)* **2012**, *246*, 60−69.
(62) Duerr-Auster, N.; Kohlbrecher, J.; Zuercher, T.; Gunde, R.; Fischer, P.; Windhab, E. Microstructure and Stability of a Lamellar Liquid Crystalline and Gel Phase Formed by a Polyglycerol Ester Mixture in Dilute Aqueous Solution. *Langmuir* **2007**, *23*, 12827−12834.
(63) Blume, A.; Gabriel, P. Lipid model membranes and biomembranes. In *Handbook of Thermal Analysis and Calorimetry*; Kemp, R. B., Ed.; Elsevier: Amsterdam, 1999.
(64) Davis, J. H. The Description of Membrane Lipid Conformation, Order and Dynamics by ^{2}H-NMR. *BBA-Rev. Biomembranes* **1983**, *737*, 117−171.
(65) Douliez, J.-P. Phase Behavior of the Palmitic Acid/Palmitin System. A ^{2}H NMR Study. *Langmuir* **2004**, *20*, 1543−1550.
(66) Terech, P.; Talmon, Y. Aqueous Suspensions of Steroid Nanotubules: Structural and Rheological Characterizations. *Langmuir* **2002**, *18*, 7240−7244.
(67) Spector, M. S.; Selinger, J. V.; Schnur, J. M. Thermodynamics of Phospholipid Tubules in Alcohol/Water Solutions. *J. Am. Chem. Soc.* **1997**, *119*, 8533−8539.
(68) Nakashima, N.; Asakuma, S.; Kunitake, T. Optical Microscopic Study of Helical Superstructures of Chiral Bilayer Membranes. *J. Am. Chem. Soc.* **1985**, *107*, 509−510.